1986

An air-ice feedback mechanism for the migration of the marginal ice zone

Chu, Peter C.

Chu, P.C., 1986: An air-ice feedback mechanism for the migration of the marginal ice zone. Marginal Ice Zone Experiment Bulletin, 7, 54-64

An Ice/Air Feedback Mechanism for the Migration of the Marginal Ice Zone

P.C. CHU
Department of Geophysical Sciences
The University of Chicago, Chicago, Illinois

The aim of this study is to investigate, by means of a coupled ice/air model, the generation of strong along-ice-edge winds in the MIZ, the formation of the ice edge jet, and the instability criteria of ice drift. Ice-drift observations in the Greenland Sea from 28 April to 3 September 1978 (Figure 1) show two different types of ice motion. Oscillation occurs mostly in spring (April, May, and June) and nonoscillation takes place in summer (July and August). Ice melts and becomes thinner from winter to summer. Although ocean eddies probably produce oscillations in drift track, another relation between the pattern of ice motion and ice thickness may still exist. One purpose of the present work is to find this relation.

A possible mechanism for the air/ice interaction is presented in Figure 2. The low-level air flow generated by differential surface heating is waterward (icebreeze) and equatorward along the ice edge in both eastern Greenland and the eastern Antarctic Peninsula and influences the ice through surface air stress. However, movement of the ice edge in the MIZ toward warm water changes the thermal conditions near the surface and produces an air surface temperature gradient across the ice edge.

The ice/air interaction model depicted in this article is intended to simulate the main physical processes and to determine some instability criteria for the prediction of MIZ migration.

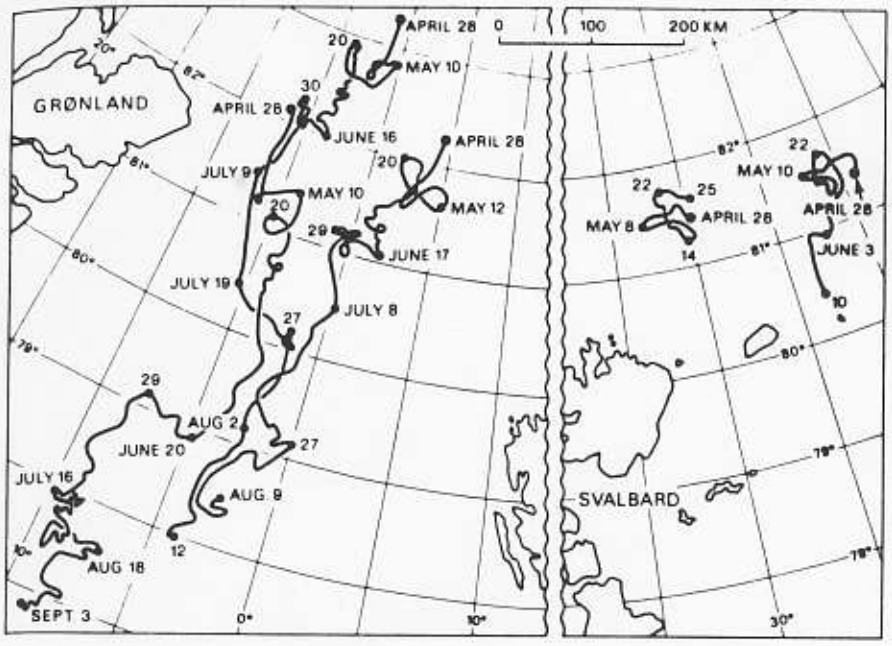

Fig. 1. Ice-drift observations in the Greenland Sea.

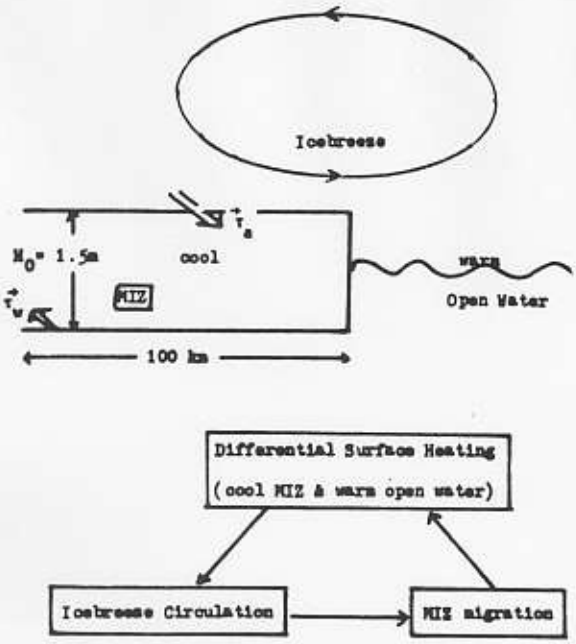

Fig. 2. Ice/air/water coupled system.

Thermally forced boundary layer air flow

The surface isotherms, which are nearly parallel to the eastern coast of Greenland over the Greenland Sea (Prik, 1959), indicate that air temperature monotonically increases waterward near the MIZ. Such differental surface heating generates a local air flow near the MIZ. In this section we utilize a planetary boundary layer model treated by Kuo (1973) and Chu (1985) to simulate a thermally forced boundary layer air flow. The coordinate system is chosen as moving with the edge of the MIZ. The x-axis is in the cross-edge direction, and the y-axis parallels the ice edge, as shown in Figure 3. The x-coordinate's unit length is twice the MIZ width, L (200 km), and that of the vertical coordinate is $\Omega = (\nu/\Omega)^{1/2}$, where ν is the vertical eddy viscosity and Ω is the angular velocity of the earth's rotation. The line $x = 1/2$ is located at the ice edge. The MIZ covers the zone $(0 < x < 0.5, y)$ where the y-axis $(x = 0)$ is near the boundary between the MIZ and the interior ice pack. It is considered that spatial variations in the MIZ are much larger perpendicular to the ice edge than parallel to it, so derivatives with respect to y are assumed to be zero. Since acceleration of the ice edge is small compared to that of the air flow, we may ignore the inertial force due to the use of a coordinate system (moving relative to the earth).

The potential temperature of air is divided into two parts: a basic state $\theta_{B*}(z)$ and perturbation θ'_*. The basic state is given by

$$\theta_{B*}(z) = \theta_{B0} + (N^2\theta_{B0}\delta/g)z, \tag{1}$$

where θ_{B0} is the basic air potential temperature at the surface and N is the Brunt–Vaisaila frequency.

Waterward migration of the MIZ increases the surface temperature gradient, and iceward migration of the MIZ decreases the surface temperature gradient. Surface temperature perturbation is parameterized as

$$\theta'_* = -DT_0[1 + \zeta(t)]\cos \pi x, \tag{2}$$

where DT_0 is the mean surface temperature difference across the MIZ and $\zeta(t)$ is the nondimensional displacement of the ice edge. The coordinates and atmospheric variables are nondimensionalized by setting

$$\begin{aligned} (x_*, z_*, t_*) &= (xL, z\delta, tT), \\ s' \equiv \theta'_*/\theta_{B0} &= (DT_0/\theta_{B0})s \\ (u_*, v_*, w_*) &= U(u, v, w\delta/L), \\ P_* &= \varrho_a(g\delta DT_0/\theta_{B0})P, \end{aligned} \tag{3}$$

where

$$U \equiv g\delta DT_0/(2L\Omega\theta_{B0}) \tag{4}$$

is the scale of the icebreeze wind and T is the time scale for the change of surface heating due to the movement of the ice edge. If we assume that the local air flow satisfies the modified Boussinesq approximation (Kuo, 1973), then the vorticity equation, the momentum equation (both in the y direction), and the heat equation for air disturbances

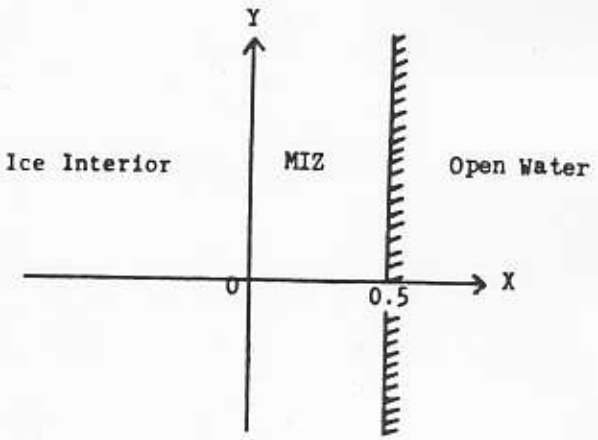

Fig. 3. The model MIZ and the coordinate system.

generated by differential heating near the MIZ are written by (Chu, 1985)

$$E\nabla_\nu^2 \nabla_\nu^2 = f_0\, \partial v/\partial z - \partial s/\partial x, \tag{5}$$

$$E\nabla_\nu^2 v = -f_0\, \partial\psi/\partial z, \tag{6}$$

$$E\nabla_\nu^2 s = R_i\, \partial\psi/\partial x, \tag{7}$$

and

$$\begin{aligned} &u = -\partial\psi/\partial z, \quad w = \partial\psi/\partial x, \\ &\nabla_\nu^2 \equiv \delta^2 \nu_h/(L^2\nu)\partial^2/\partial x^2 + \partial^2/\partial z^2, \\ &\nabla^2 \equiv \delta^2/L^2\, \partial^2/\partial x^2 + \partial^2/\partial z^2 \doteq \partial^2/\partial z^2, \end{aligned} \tag{8}$$

where $f_0 = \sin\lambda$, λ is the latitude, and

$$E \equiv \nu/(2\Omega\delta^2) = \tfrac{1}{2}, \quad R_i \equiv \delta^2 N^2/(4L^2\Omega^2) \tag{9}$$

are the Ekman number and global Richardson number, respectively. Eliminating v and s from Equations 5 through 7, we find that the streamfunction satisfies the following partial differential equation:

$$(\tfrac{1}{4}\nabla_\nu^4 + f_0^2)\, \partial^2\psi/\partial z^2 + R_i\, \partial^2\psi/\partial x^2 = 0. \tag{10}$$

We solve Equation 10 for streamfunction ψ, and obtain the solutions of v and s from Equations 6 and 7 after substituting ψ. The local air flow is thermally forced by differential surface heating as indicated in Equation 2; therefore, the streamfunction should be written as

$$\psi(x, z, t) = \bar{\psi}(z, t) \sin\pi x. \tag{11}$$

The boundary conditions in the vertical direction are derived as follows. The dependent variables should remain finite as $z \to \infty$, i.e.,

$$\lim_{z\to\infty} (|\psi|, |\partial\psi/\partial z|, |v|, |s|) < \infty. \tag{12}$$

The boundary conditions at $z = 0$ are:

$$\begin{aligned} &\psi = 0, \qquad \partial\psi/\partial z = K\partial^2\psi/\partial z^2, \\ &v = K\partial v/\partial z, \qquad s = -[1 + \zeta(t)] \cos\pi x, \end{aligned} \tag{13}$$

where K is a measure of the effective depth of the constant stress-sublayer (Kuo, 1971). Substituting Equation 11 into Equation 10 we obtain the following sixth-order ordinary differential equation for the Fourier coefficient $\bar{\psi}$:

$$\begin{aligned} &d^6\bar{\psi}/dz^6 - 4\gamma d^4\bar{\psi}/dz^4 + 4(f_0^2 + \gamma^2) \\ &\quad d^2\bar{\psi}/dz^2 - 4\pi^2 R_i\bar{\psi} = 0 \end{aligned} \tag{14}$$

where

$$\gamma \equiv \pi^2\delta^2\, \nu_h/(2L^2\nu). \tag{15}$$

The general solution of Equation 14 has the following form:

$$\bar{\psi}(z, t) = [1 + \zeta(t)] \sum_{j=1}^{6} \bar{a}_j e^{\lambda_j z}, \tag{16}$$

where the eigenvalues λ_j ($j = 1,2,\ldots,6$) are the roots of the succeeding sixth-order algebraic equation:

$$\lambda^6 - 4\gamma\lambda^4 + 4(f_0^2 + \gamma^2)\lambda^2 - 4\pi^2 R_i = 0. \tag{17}$$

Table 1 lists all the eigenvalues under typical stratification at three distinct latitudes (65°, 70°, and 75°). Notice that f_0^2 appears in Equation 17, so the eigenvalues in Table 1 represent both northern and

Table 1. The eigenvalues of the boundary layer air flow model at three different latitudes.

Latitude		
65°	*70°*	*75°*
(-0.32371, 0)	(-0.31223, 0)	(-0.30378, 0)
(-1.02800, 0.87796)	(-1.04508, 0.89586)	(-1.05823, 0.90973)
(-1.02800, -0.87796)	(-1.04508, -0.89586)	(-1.05823, -0.90973)
(0.32371, 0)	(0.31223, 0)	(0.30378, 0)
(1.02800, 0.87796)	(1.04508, 0.89586)	(1.05823, 0.90973)
(1.02800, -0.87796)	(1.04508, -0.89586)	(1.05823, -0.90973)

southern polar regions. According to the upper boundary conditions listed in Equation 12 we must set up coefficients that correspond to those eigenvalues with positive real parts to zero. Consequently the general solution Equation 16, satisfying the top boundary conditions, may be written by:

$$\bar{\psi}(z, t) = [1 + \zeta(t)] \sum_{j=1}^{3} \bar{a}_j e^{\lambda_j z}, \tag{18}$$

where the eigenvalues λ_j all have the negative real parts. Substituting Equation 18 into 11 we obtain the streamfunction

$$\psi(x, z, t) = \sum_{j=1}^{3} \bar{a}_j [1 + \zeta(t)] e^{\lambda_j z} \sin \pi x. \tag{19}$$

Integrating the momentum equation (6) and heat equation (7) with respect to z after substituting Equation 19, we find that v and s are given by

$$v(x, z, t) = [\bar{b} e^{-\sqrt{2\gamma} z} - f_0 \sum_{j=1}^{3} \bar{a}_j \lambda_j F(\lambda_j, \gamma) e^{\lambda_j z}][1 + \zeta(t)] \sin \pi x, \tag{20}$$

$$s(x, z, t) = [\bar{c} e^{-\sqrt{2\gamma} z} + \pi R_i \sum_{j=1}^{3} \bar{a}_j F(\lambda_j, \gamma) e^{\lambda_j z}][1 + \zeta(t)] \cos \pi x. \tag{21}$$

where

$$F(\lambda, \gamma) \equiv 1/(\lambda^2/2 - \gamma). \tag{22}$$

Substituting solutions 19–21 into the vorticity equation (5) we find that

$$\bar{c} = \sqrt{2\gamma} f_0 \bar{b}/\pi. \tag{23}$$

Substituting solutions 19–21 into the surface boundary conditions listed in Equation 13, we obtain the following four algebraic equations for $\bar{a}_j$ and $\bar{b}$.

$$\sum_{j=1}^{3} \bar{a}_j = 0 \tag{24}$$

$$\sum_{j=1}^{3} \lambda_j (1 - K\lambda_j) \bar{a}_j = 0 \tag{25}$$

$$-f_0 \sum_{j=1}^{3} \lambda_j (1 - K\lambda_j) F(\lambda_j, \gamma) \bar{a}_j + \bar{b}(1 + K\sqrt{2\gamma}) = 0 \tag{26}$$

$$\pi R_i \sum_{j=1}^{3} F(\lambda_j, \gamma) \bar{a}_j + \sqrt{2\gamma} f_0 \bar{b}/\pi = -1. \tag{27}$$

The four constants $\bar{a}_1$, $\bar{a}_2$, $\bar{a}_3$, and $\bar{b}$ can be readily obtained by solving the four linear nonhomogeneous algebraic equations.

Figures 4–6 reveal the solutions for zero ice motion at $\lambda = 75°$, $DT_0 = 6$ °C, and $N = 10^{-2}$ s^{-1}. Figure 4 shows the distribution of air temperature

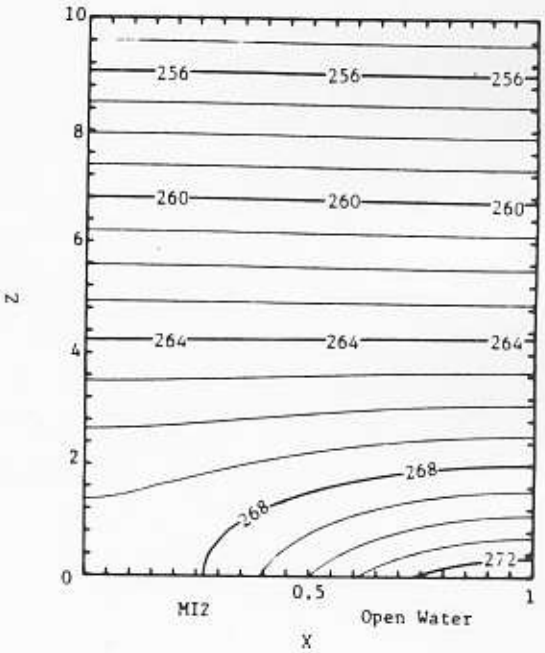

Fig. 4. The distribution of air temperature (°K) in the cross-ice section.

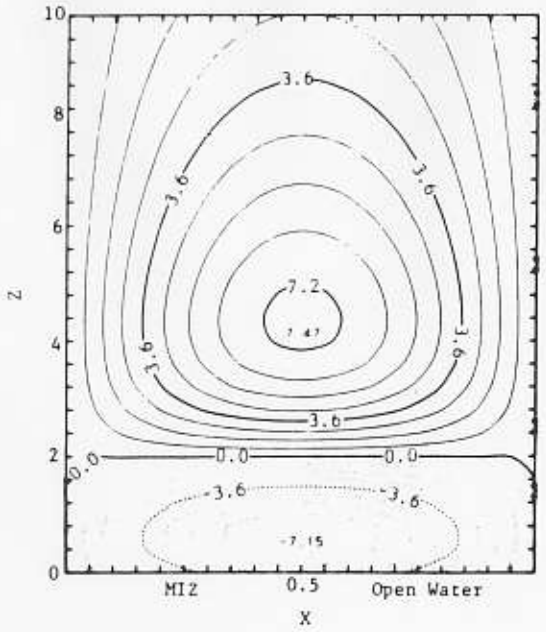

Fig. 5. The distribution of thermally forced along-ice-edge winds (m s^{-1}) in the cross-ice section.

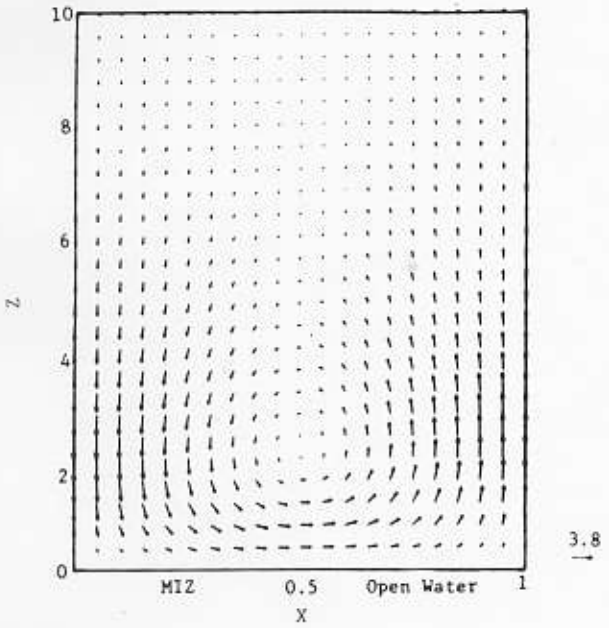

Fig. 6. Thermally forced icebreeze circulation in the cross-ice section with u *in m s^{-1} and* w *in cm s^{-1}.*

in the cross-ice section. The horizontal temperature gradient is very deep near the ice edge and decreases with altitude. Above $z = 3$ ($z_* = 800$ m) there is almost no horizontal temperature gradient. Figure 5 shows the distribution of the wind along ice-edge v in the cross-ice section. The longshore wind is equatorward at low levels (below $z = 2$) and poleward at high levels. This strong equatorward wind along the ice edge near the MIZ (around 7 m s^{-1}) is consistent with the observations along the eastern Antarctic Peninsula (Schwerdtfeger, 1979). Figure 6 shows the cross-ice circulation. The maximum value of the ice breeze, which is around 3 m s^{-1}, is located at the ice edge.

Ice drift model

Suppose that the MIZ is considered to be pack ice with linear viscous rheology and constant shear and bulk viscosities. The MIZ has a mean thickness of H_0. The linearized momentum equation and continuity equation are written by:

$$\partial u_i/\partial t_* = (\bar{\xi}+\bar{\eta})\,\partial^2 u_i/\partial x^2 + fv_i + (\tau_{ax}+\tau_{wx})/(\varrho_i H_0) - g\partial h_i/\partial x, \quad (28)$$

$$\partial v_i/\partial t_* = \bar{\eta}\,\partial^2 v_i/\partial x^2 - fu_i + (\tau_{ay}+\tau_{wy})/(\varrho_i H_0) \quad (29)$$

$$\partial h_i/\partial t_* = -(H_0/L)\,\partial u_i/\partial x, \quad (30)$$

where $f(=2\Omega\sin\lambda)$ = Coriolis parameter
ϱ_i = ice density
u_i, v_i = $\mathbf{V}_i$, ice velocity
τ_{ax}, τ_{ay} = τ_a, wind stress
τ_{wx}, τ_{xy} = τ_w, water stress
h_i = ice thickness perturbation generated by forcing terms
x = nondimensional horizontal coordinate

and $\bar{\eta}$ and $\bar{\xi}$ are defined by

$$\bar{\xi} \equiv \xi/(\varrho_i H_0 L^2), \qquad \bar{\eta} \equiv \eta/(\varrho_i H_0 L^2), \quad (31)$$

where η and ξ are the shear and bulk viscosities of ice. The air and water stresses are given by

$$\tau_a = C_a' \mathbf{V}_a, \quad (32)$$

$$\tau_w = C_w'(\mathbf{V}_w - \mathbf{V}_i), \quad (33)$$

where $\mathbf{V}_a$ is the surface air velocity, $\mathbf{V}_w$ the surface water velocity, and C_a' and C_w' the dimensional air and water drag coefficients. C_a' is further given by

$$C_a' = C_a \varrho_a U[(\partial \psi_0/\partial z)^2 + v_0^2]^{1/2}|_{z=0,\,x=0.5}, \quad (34)$$

where ψ_0 and v_0 are obtained by Equations 19 and 20. In contrast to the treatments by Hibler (1984), Lepparanta and Hibler (1984), and Lepparanta (1984), the surface air and water stresses τ_a and τ_w are directly computed by the boundary layer flow model presented in the previous section. Substituting the expressions for air and water stresses (32) and (33) into Equations 28 and 29 and assuming that $\mathbf{V}_w = 0$, we obtain

$$\partial u_i/\partial t_* = (\bar{\xi} + \bar{\eta})\,\partial^2 u_i/\partial x^2 - \bar{C}_w u_i + f v_i$$
$$\bar{C}_a u_{a0}[1 + \zeta(t)] \sin \pi x - g/L\,\partial h_i/\partial x, \quad (35)$$

$$\partial v_i/\partial t_* = \bar{\eta}\partial^2 v_i/\partial x^2 - \bar{C}_w v_i - f u_i$$
$$+ \bar{C}_a v_{a0}[1 + \zeta(t)] \sin \pi x, \quad (36)$$

where

$$\bar{C}_a \equiv C_a'/(\varrho_i H_0), \qquad \bar{C}_w \equiv C_w'/(\varrho_i H_0),$$

$$u_{a0} \equiv -g\delta DT_0/(2L\Omega\theta_{B0}) \sum_{j=1}^{3} \bar{a}_j \lambda_j,$$

$$v_{a0} \equiv g\delta DT_0/(2L\Omega\theta_{B0})[\bar{b} - f_0 \sum_{j=1}^{3} \bar{a}_j \lambda_j F(\lambda_j, \gamma)]. \quad (37)$$

Equations 30, 35, and 36 are the basic equations for ice motion. The solutions of these two equations should have the same Fourier component as the forcing terms, i.e.,

$$u_i(x, t_*) = \bar{u}_i(t_*) \sin \pi x,$$
$$v_i(x, t_*) = \bar{v}_i(t_*) \sin \pi x. \quad (38)$$

By definition, $\zeta(t)$ is the nondimensional ice-edge displacement in the x-direction. It is related to ice velocity by

$$L d\zeta/dt_* = u_i(1/2, t_*) = \bar{u}_i(t_*). \quad (39)$$

Eliminating two of the three dependent variables, u_i, v_i, and h_i, from Equations 30, 35, and 36 we get the following third-order equation for the coefficients:

$$[D^3 + (\alpha_1 + \alpha_2)D^2 + (\pi^2 g H_0/L^2 - \bar{C}_a u_{a0}/L$$
$$+ \alpha_1\alpha_2 + f^2)D + \alpha_2(\pi^2 g H_0/L^2 - \bar{C}_a u_{a0}/L)$$
$$- f\bar{C}_a v_{a0}/L](\bar{u}_i, \bar{v}_i) = 0, \quad (40)$$

where

$$D = d/dt_*,$$
$$\alpha_1 \equiv \pi^2(\bar{\xi} + \bar{\eta}) + \bar{C}_w,$$
$$\alpha_2 \equiv \pi^2 \bar{\eta}^2 \bar{C}_w \quad (41)$$

The general solutions of Equation 40 have the following form:

$$\bar{u}_i(t_*) = \sum_{j=1}^{3} d_j \exp(\mu_j t_*),$$
$$\bar{v}_i(t_*) = \sum_{j=1}^{3} e_j \exp(\mu_j t_*). \quad (42)$$

The eigenvalues μ_1, μ_2, μ_3 are the roots of the following equation:

$$\mu^3 + (\alpha_1 + \alpha_2)\mu^2$$
$$+ (\pi^2 g H_0/L^2 - \bar{C}_a u_{a0}/L + \alpha_1\alpha_2 + f^2)\mu$$
$$+ \alpha_2(\pi^2 g H_0/L^2 - \bar{C}_a u_{a0}/L) - f\bar{C}_a v_{a0}/L = 0. \quad (43)$$

Stability and oscillation criteria

In the present research the bulk ice viscosity ξ is taken to be twice the shear ice viscosity η. The standard values of the parameters are given in Table 2. We solve the characteristic equation (43) with different values of H_0, η, and DT_0. H_0 varies from 0.5 to 10.5 m, η from 0 to 2×10^9 kg s^{-1}, and DT_0 from 1 °C to 21 °C. The instability criterion of the MIZ migration in the ice/air-coupled model can be written by

$$\mathrm{Re}(\bar{\mu}) \begin{cases} < 0 \text{ decaying} \\ = 0 \text{ neutral} \\ > 0 \text{ growing} \end{cases} \qquad \bar{\mu} = \mu_1, \mu_2, \mu_3 \quad (44)$$

Table 2. The standard model parameters.

$L = 200$ km	$\nu = 5\ \mathrm{m^2\ s^{-1}}$	$\nu_h = 10^3\ \mathrm{m^2\ s^{-1}}$
$\Omega = 0.729\times10^{-4}\ \mathrm{s^{-1}}$	$g = 9.81\ \mathrm{m^2\ s^{-2}}$	$K = 0.9$
$N = 10^{-2}\ \mathrm{s^{-1}}$	$\theta_{B0} = 270\,^{\circ}\mathrm{K}$	$C_w' = 0.55\ \mathrm{kg/m^2\ s^{-1}}$
$C_a' = 1.2\times10^3$	$\varrho_a = 1.29\ \mathrm{kg\ m^3}$	$\varrho_w = 10^3\ \mathrm{kg\ m^3}$
$\varrho_i = 910\ \mathrm{kg\ m^3}$	$U_i < 1\ \mathrm{m\ s^{-1}}$	$\lambda = (65^{\circ},70^{\circ},75^{\circ})$

where $\bar{\mu}$ is the root of the cubic equation (43). The oscillation criterion of the MIZ migration is given by

$$\mathrm{Im}(\bar{\mu}) \begin{cases} = 0 & \text{nonoscillatory} \\ \neq 0 & \text{oscillatory} \end{cases} \qquad \bar{\mu} = \mu_1, \mu_2, \mu_3 \quad (45)$$

Dependence of eigenvalues on parameters

We compute all the roots of Equation 43. Here μ_1 is real in the entire space, and μ_2 and μ_3 are real for some values of (H_0, η, DT_0) and are complex conjugates for others.

Figure 7 shows the surface of $\mu_1 = 0$ in three-dimensional space (H_0, η, DT_0). This surface divides the space into two parts corresponding to growing and decaying modes. The growing mode appears when DT_0 exceeds some critical value around 2 °C, and is located in the small mean ice-thickness H_0 region. Ice motion corresponding to the eigenvalue μ_1 is nonoscillatory.

Figure 8 indicates the surface of $\mathrm{Re}(\mu_2) = 0$ [or

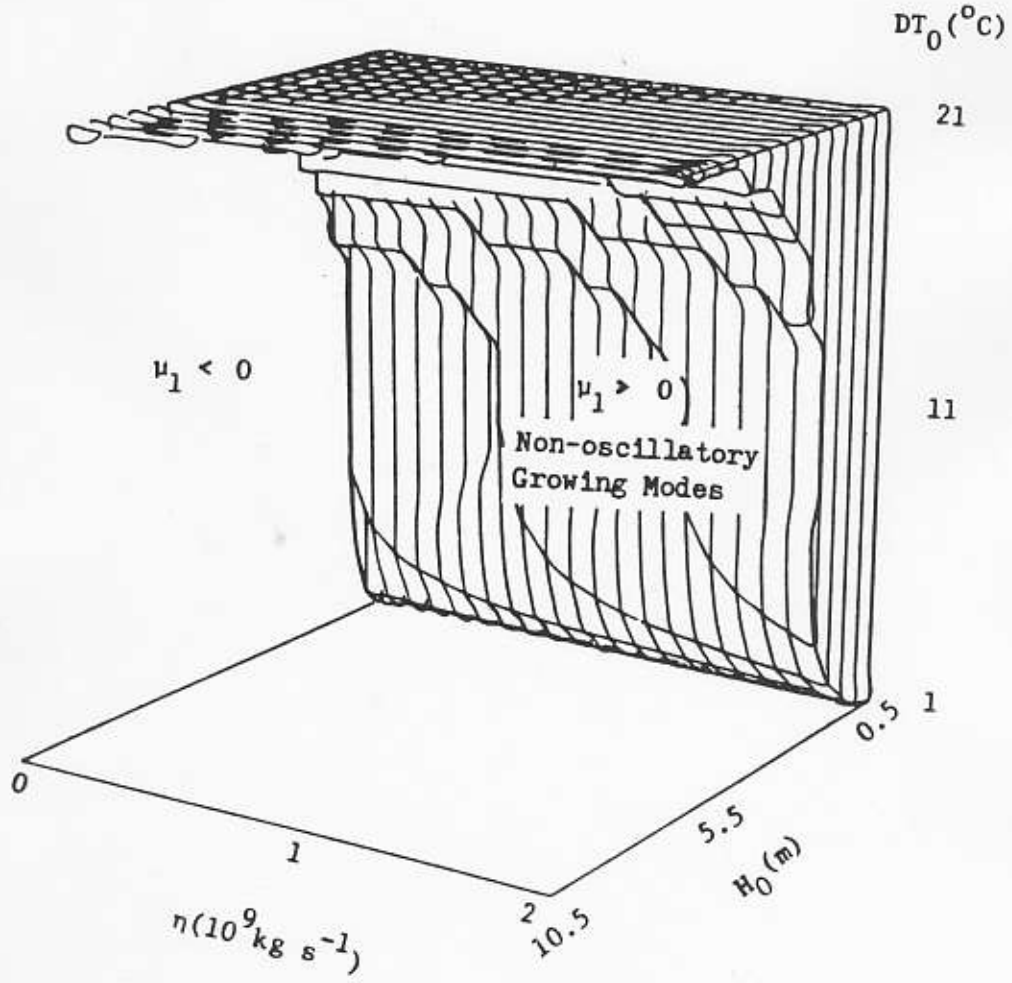

Fig. 7. Separation of nonoscillatory decaying and growing modes referring to real eigenvalue μ_1.

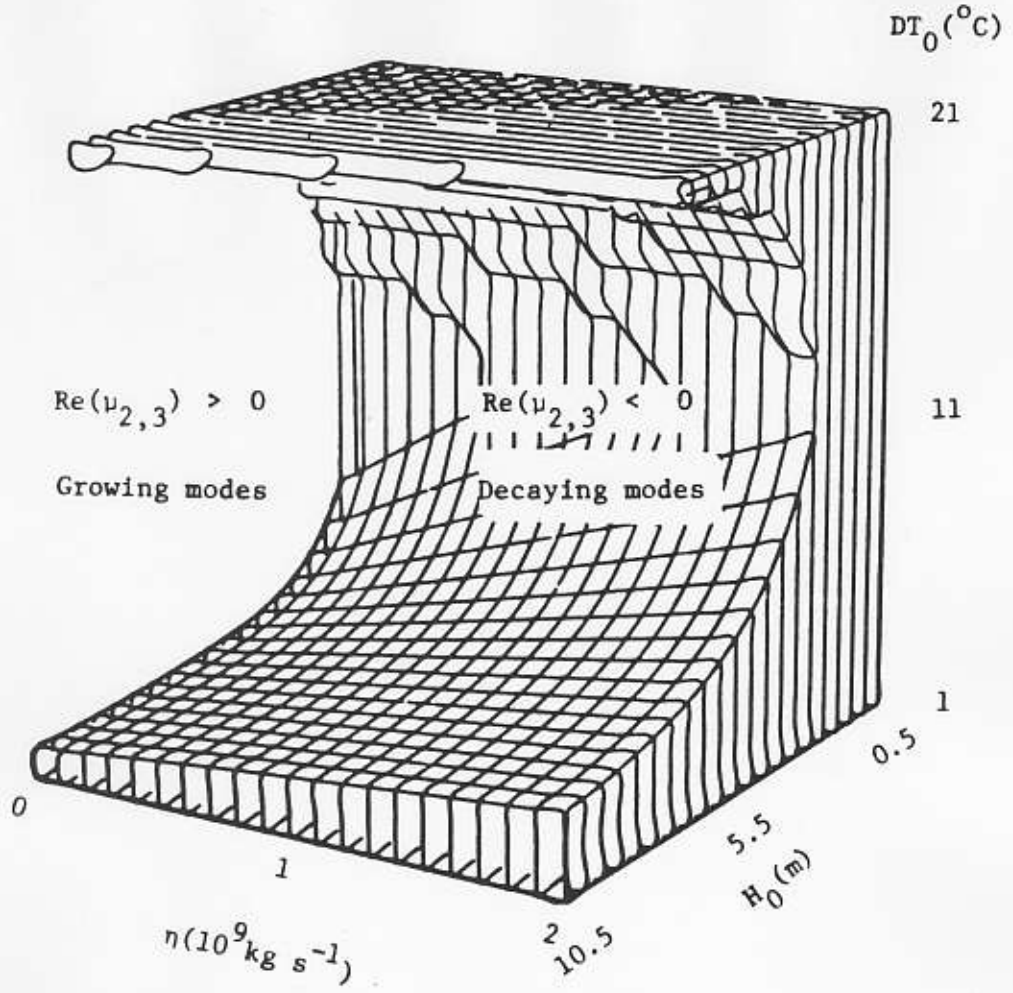

Fig. 8. Separation of decaying and growing modes referring to eigenvalues μ_2 and μ_3.

$\mathrm{Re}(\mu_i) = 0$] in the parameter space (H_0, η, DT_0). This surface separates the whole space into growing and decaying parts. The growing mode is present when DT_0 exceeds some critical value that is a function of H_0 and η (in case of $H_0 = 4.5$ m and $\eta = 10^9$ kg s^{-1}, $DT_0 = 6$ °C), and is concentrated in the large mean ice-thickness H_0 region.

Figure 9 reveals the segregation of nonoscillatory and oscillatory modes relating to μ_2 and μ_3. Comparing Figure 9 with Figure 8, we find that the decaying mode of μ_2 and μ_3 is nonoscillatory, whereas the growing mode of μ_2 and μ_3 is oscillatory.

Whether ice motion grows or decays substantially depends on the parameter DT_0. When DT_0 is small, the motive force is so small that it cannot overcome the dissipative effect and does not make ice motion unstable. If DT_0 becomes large enough to overcome the dissipative forces originated by ice stress and friction, ice motion becomes larger.

Whether ice motion is oscillatory or nonoscillatory largely depends on parameter H_0. In cases of small H_0, the restoring force is so small that it cannot balance the motive force and cannot produce oscillations. However, when parameter H_0 exceeds some critical value (which varies with DT_0 and η) and becomes large enough to balance the motive force brought on by the ice breeze generated by surface temperature difference, the ice motion becomes oscillatory.

For the nonoscillatory growing mode, the time during which ice doubles its speed is computed by

$$T_1 = \ln 2/\mu_1 \qquad (\mu_1 > 0). \tag{46}$$

If H_0, η, and ξ are assigned as commonly used values:

$$H_0 = 1.5\ \mathrm{m}, \quad \eta = 10^9\ \mathrm{kg\,s^{-1}}, \quad \xi = 2\times10^9\ \mathrm{kg\,s^{-1}},$$

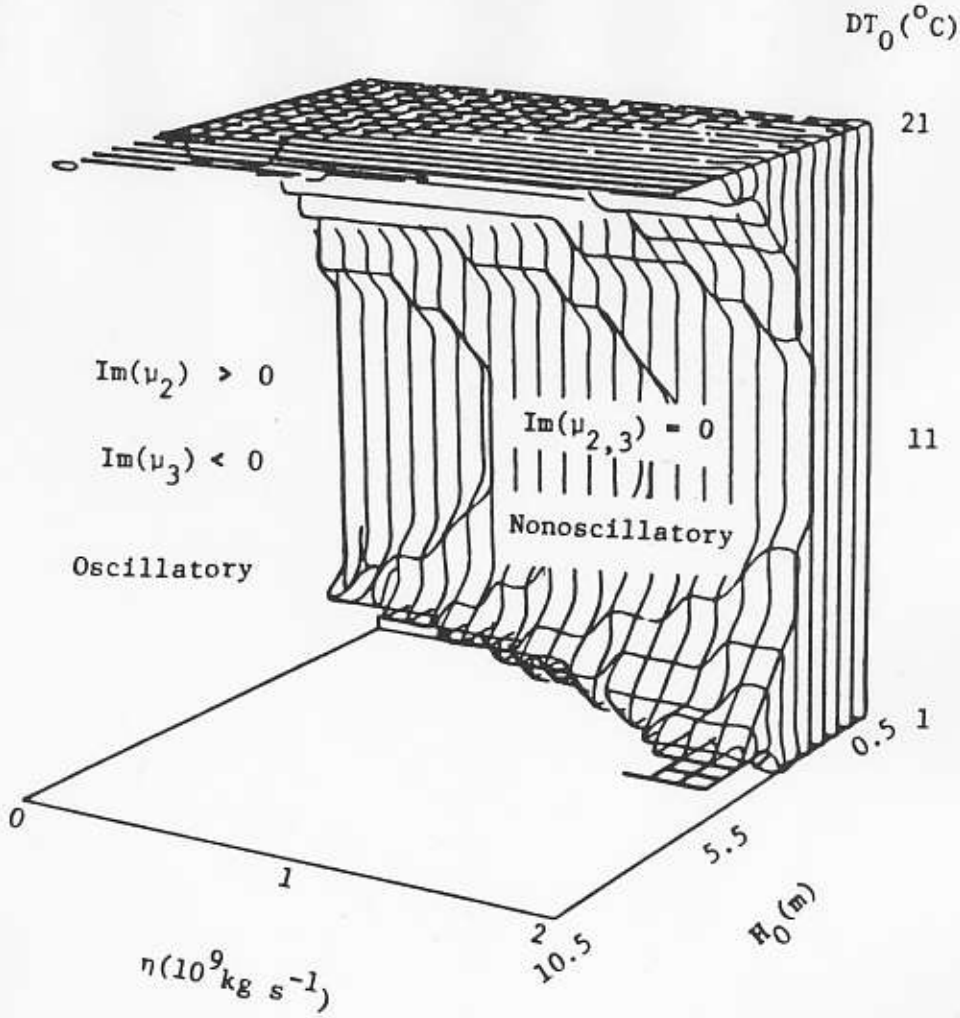

Fig. 9. Separation of nonoscillatory and oscillatory states referring to eigenvalues μ_2 and μ_3.

The doubling time treated as a function of DT_0 is shown in Figure 10, which displays a decrease of T_1 with an increase of DT_0. T_1 changes from 7.3 hr to 0.73 hr as DT_0 varies from 6 °C to 16 °C. It takes only 12.4 hr for the ice velocity to increase from 6 cm s^{-1}, which is a steady-state estimation, to 20 cm s^{-1} when $DT_0 = 6$ °C.

The oscillatory growing mode is ice motion due to μ_2 (or μ_3), whose real part is positive.

$$\mathrm{Re}(\mu_2) = \mathrm{Re}(\mu_3) > 0,$$

the growth rate $\mathrm{Re}(\mu_{2,3})$ increases with an increase of DT_0 (increase of forcing term), with an enlargement of H_0 (increase of restoring force), and with a reduction of η (decrease of dissipation). With $DT_0 = 6$°C, $\eta = 10^9$ kg s^{-1}, and $H_0 = 4.5$ m, the growth rate is 0.22×10^{-4} s^{-1} and the corresponding doubling time is 8.75 hr. The period of growing oscillatory mode, defined by

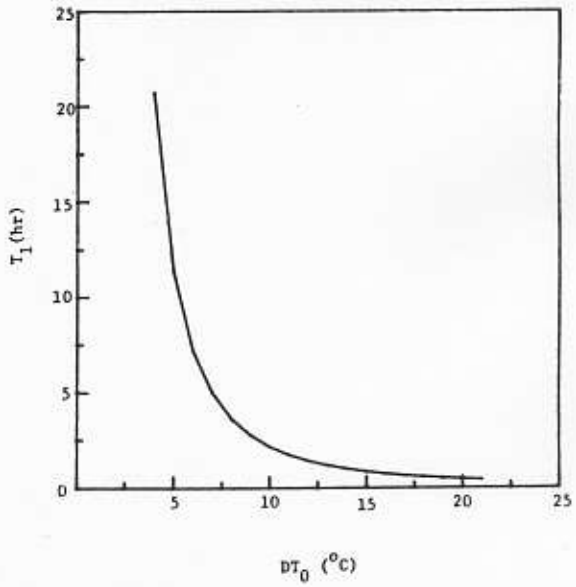

Fig. 10. Dependency of doubling time on DT_0 *for the nonoscillatory growing mode.*

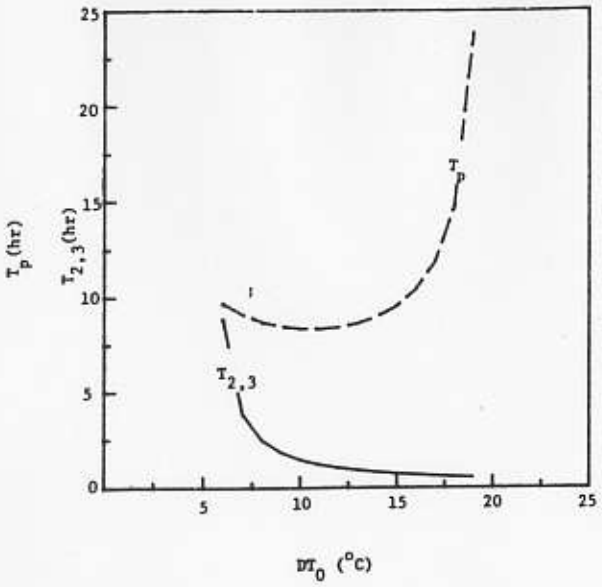

Fig. 11. Dependency of doubling time and period on DT_0 *for oscillatory growing mode.*

$$T_p = 2\pi/|\mathrm{Im}(\mu_{2,3})| \tag{47}$$

is 9.7 hr.

Figure 11 shows the growth rate and period as functions of DT_0 for H_0 = 4.5 m and $\eta = 10^9$ kg s^{-1}. The growth rate decreases monotonically with an increase of DT_0. However, the period decreases slightly when DT_0 varies from 6 °C to 10 °C, and then increases with DT_0 rapidly. When DT_0 = 19 °C, the period is nearly one day.

Conclusion

This ice/air-coupled model is intended only to depict the mesoscale processes of ice/air interaction in the MIZ. The synoptic scale pressure gradient associated with the semi-permanent Icelandic low may in addition produce equatorward winds in the Greenland Sea, and large-scale ocean currents near the East Greenland Sea or the Antarctic Peninsula may drive ice drift. These processes are, however, beyond the scope of the current research. Nevertheless, when the ice to open water temperature gradient is strong, the mesoscale feedback mechanism discussed here may become as strong, or stronger, than the synoptic scale and oceanic forcings.

The equatorward and waterward surface winds near the MIZ in the Greenland Sea and the east Antarctic Peninsula are thermally generated by differential surface heating over ice and water. The surface wind has its maximum speed along the ice edge. The component of surface wind parallel to the ice edge can reach 7 m s^{-1} when the temperature gradient in the cross-ice direction is chosen as 0.03 °K km^{-1}. This agrees with the observational results at the east Antarctic Peninsula reported by Schwerdtfeger (1979).

The migration of the MIZ is forced by local winds generated by differential surface heating over ice and water near the ice edge. The ice velocity $\mathbf{V}_i$ has sinusoidal forms (38), showing an ice edge jet. The ice velocity has its maximum at the ice edge and decreases iceward. This implies that the ice edge jet is produced indirectly by the thermal effect of the ice/water contrasts.

The ice motion has two bifurcations. It first bifurcates into decaying and growing modes, depending on th mean surface temperature difference over ice and water, DT_0. When DT_0 is small, the decaying mode predominates. However, when DT_0 exceeds some critical value (i.e., 6 °C as H_0 = 4.5 m and $\eta = 10^9$ kg s^{-1}, and 2 °C as H_0 = 1.5 m and $\eta = 10^9$ kg s^{-1}), the growing mode appears. The growing mode further bifurcates into nonoscillatory and oscillatory states, depending on ice properties. In cases of small ice thickness, which causes an inadequate restoring force and generally occurs in summer, the ice motion is nonoscillatory. In cases of large ice thickness, which generates an adequate restoring force and is usually present in winter, the ice motion is oscillatory.

This research provides a possible way to predict the MIZ migration. The procedure is as follows:

a) Observe surface temperature difference DT_0 and determine the ice properties, i.e., H_0 and η.

b) Use Figures 8 and 9 to determine the pattern of motion, i.e., growing or decaying, oscillatory or nonoscillatory, etc.

c) Employ Figures 10 and 11 to determine the growth rate and period (in case of the oscillatory state).

d) Observe initial ice velocity.

e) Make a prediction of MIZ migration according to the initial ice velocity, growth rate, and period (for the oscillatory state).

The author is grateful to Prof. H.L. Kuo and Prof. D.R. MacAyeal of the University of Chicago for invaluable discussion and comments. The reviewers' comments are also highly appreciated.

This research was supported by grant ATM 83-14206 from the National Science Foundation.

REFERENCES

Brown, R.A., Planetary boundary layer modeling for AIDJEX. In *Sea Ice Processes and Models.*

University of Washington Press, 387–401, 1980.

Chu, P.C., A boundary layer theory of coastal desert formation and seabreeze circulation. Ph.D. thesis, The University of Chicago, 194 pp., 1985.

Glen, J.W., Thoughts on a viscous model for sea ice. *AIDJEX Bull., 2,* 18–27., 1970.

Hibler, W.D., III, Ice dynamics. CRREL Monograph 84-3, 52 pp., 1984.

Kuo, H.L., Axisymmetric flows in the boundary layer of a maintained vortex. *J. Atmos. Sci., 28,* 20–41, 1971.

Leavitt, E., Surface-based air stress measurements made during AIDJEX. In *Sea Ice Processes and Models.* University of Washington Press, 419–429, 1980.

Lepparanta, M. and W.D. Hibler III, On the role of ice interaction in marginal ice zone dynamics. *MIZEX Bulletin III,* USA Cold Regions Research and Engineering Laboratory, Special Report 84-7, pp. 23–29, 1984.

Macklin, S.A., Wind drag coefficient over first-year sea ice in the Bering Sea. *J. Geophys. Res., 88,* 2845–2952, 1983.

McPhee, M.G., The effect of the oceanic boundary layer on the mean drift of pack ice: Application of a simple model. *J. Phys. Oceanogr., 9,* 388–400, 1979.

Overland, J.E., H.O. Mofjeld and C.H. Pease, Wind-driven ice drift in a shallow sea. *MIZEX Bulletin III,* USA Cold Regions Research and Engineering Laboratory, Special Report 84-7, pp. 49–53, 1984.

Pease, C.H., S.A. Salo, and J.E. Overland, Drag measurements for first-year sea ice over a shallow sea. *J. Geophys. Res., 88,* 2853–2862, 1983.

Prik, Z.M., Mean position of surface pressure and temperature distribution in the Arctic. *Tr. Arkticheskogo Nauchn.-Issled. Inst., 217,* 5–24 (in Russian), 1959.

Schwerdtfeger, W., Meteorological aspects of the drift of ice from the Weddell Sea toward the mid-latitude westerlies. *J. Geophys. Res., 84,* 6321–6328, 1979.

Smith, S.D., E.G. Banke, and O.M. Johannessen, Wind stress and turbulence over ice in the Gulf of St. Lawrence. *J. Geophys. Res., 75,* 2803–2812, 1970.

Vinje, T.E., The drift pattern of sea ice in the Arctic with particular reference to the Atlantic approach. In *The Arctic Ocean,* John Wiley and Sons, New York, 83–96, 1982.